FULL PAPER

Dynamic Control Over Electronic Transport in 3D Bulk Nanographene via Interfacial Charging

Subho Dasgupta, Di Wang, Christian Kübel, Horst Hahn, Theodore F. Baumann, and Jürgen Biener**

Electrochemical surface charge-induced variation of physical properties in interface-dominated bulk materials is a rapidly emerging field in material science. The recently developed three-dimensional bulk nanographene (3D-BNG) macro-assemblies with ultra-high surface area and chemical inertness offer new opportunities in this area. Here, the electronic transport in centimeter-sized 3D-BNG monoliths can be dynamically controlled via electrochemically induced surface charge density. Specifically, a fully reversible variation in macroscopic conductance up to several hundred percent is observed with ≤1 V applied gate potential. The observed conductivity change can be explained in the light of the electrochemically-induced accumulation or depletion of charge carriers in combination with a large variation in the carrier mobility; the latter, being highly affected by the defect density modulations resulting from the interfacial charge injection, sharply decreases with an increase in defect concentrations. The phenomenon presented in this study is believed to open the door to novel applications of bulk graphene materials such as, for example, low voltage and high power tunable resistors.

1. Introduction

Although surface charge induced variations in material properties have been well known for many years,[1–4] they have recently attracted renewed research interest.[5–11] In fact, dynamic control of electronic transport in semiconducting thin films by means of strong perpendicular electric fields is the underlying principle of the field-effect transistor (FET) device that has revolutionized our society.[1–3] The length scale over which the external electric field can be screened inside a material by its mobile charge carriers is known as 'Debye length' (l_D) which is a function of the charge carrier concentration. Metals, for example, possess a large carrier density (>10^{22}/cm^3) that effectively screens an applied electric field at the very surface atomic layer. Consequently, efforts to measure field-induced changes of properties in high conducting materials have not been made, until very recently, when metallic materials with extremely large surface-to-volume (S/V) ratios have become available to surmount the problem associated with short screening lengths.[5–11]

Even in case of semiconductors that have orders of magnitude lower carrier concentration than metals, it is only a few hundred nanometer thick surface layer that is affected by externally applied electric fields.[1–3] This makes it difficult to induce measurable field induced changes in the properties of bulk materials. However, it has recently been shown that dynamic control over macroscopic properties in bulk materials, even for metals, becomes possible by filling the pores of nanoporous bulk materials with an electrolyte and using the so-called electrolyte-gating approach.[12] In this case, electrochemical polarization of the electrode/electrolyte interface creates large interfacial electric fields by the formation of a parallel plate capacitor-like electric double layer (EDL) which by its nature is conformal to any given morphology of the nanoporous bulk electrode. Therefore, by filling the pores of a nanoporous bulk material with an electrolyte and applying the concept of electrolyte gating, it becomes possible to generate strong electric fields at the solid/electrolyte interface throughout the entire volume of a bulk electrode. Due to the nanometer-size dimensions of the EDL, the generated electric field can be as high as 10^7 V/cm even if the applied gate potential is less than 1 V. The resulting interfacial capacitance of electrochemically gated interfaces can thus reach values as high as several tens of μF/cm^2, which allows one to realize large changes in the charge carrier density even at small applied gate potentials.

Dr. S. Dasgupta, Dr. D. Wang, Dr. C. Kübel, Prof. H. Hahn
Institute for Nanotechnology
Karlsruhe Institute of Technology (KIT)
76344, Eggenstein-Leopoldshafen, Germany
E-mail: subho.dasgupta@kit.edu
Dr. S. Dasgupta, Dr. T. F. Baumann, Dr. J. Biener
Nanoscale Synthesis and Characterization Laboratory
Lawrence Livermore National Laboratory
7000 East Ave, Livermore, CA 94550, USA
E-mail: biener2@llnl.gov
Dr. D. Wang, Dr. C. Kübel
Karlsruhe Nano Micro Facility
Karlsruhe Institute of Technology (KIT)
76344, Eggenstein-Leopoldshafen, Germany
Prof. H. Hahn
KIT-TUD Joint Research Laboratory Nanomaterials
Technische Universität Darmstadt (TUD)
Institute of Materials Science
Petersenstr. 32 64287, Darmstadt, Germany
Prof. H. Hahn
Helmholtz Institute Ulm
Albert-Einstein-Allee 11 89081, Ulm, Germany

DOI: 10.1002/adfm.201303534

Technological developments in the electrolyte-gated bulk material systems, however, are limited by the availability of suitable materials that combine an ultra-high surface area with electrochemical and mechanical stability, ideally at low cost. So far, most studies have utilized nanoporous gold (np-Au)[13,14] despite the fact that the S/V ratio of np-Au does not exceed 20% even when the feature/ligament size is reduced to 5 nm.[15] Furthermore, np-Au tends to coarsen in presence of electrolytes, especially if it is electrochemically cycled, thereby further reducing the S/V ratio.[16] In search for a material that is more stable than np-Au and exhibits a higher S/V ratio, we have tested a recently developed sol-gel polymer-derived bulk nanographene (BNG) material that is mass-producible, mechanically robust, highly conductive (3.5 S/cm) and, most importantly, possess an ultra-high surface area (1500–3000 m^2/g). In addition, the material exhibits high electrochemical inertness and a specific capacitance in excess of 125 F/g. Adding to its merits, BNG monoliths can be fabricated in any desired size and shape; the porosity, specific surface area, pore size distribution and bulk density of the material can be determinsitically controlled by activation in CO_2.

Electrolyte-gating of its fundamental building block, graphene, has already been demonstrated in graphene field-effect transistors (GFETs)[17–20] where the reported low On/Off ratio (<10) can be explained by the metallic conductivity and an absence of a band gap in graphene. In our study, we observed completely reversible conductivity variations of comparable magnitude (>400%) in centimeter-sized BNG monoliths. In bulk materials, even a low On/Off ratio may be of technological importance as a bulk transistor could support gate-controlled extraordinarily large currents flowing through the metallic bulk channel. The combination of the high intrinsic conductivity of BNG electrodes and a relatively large electrolyte-gated conductivity modulation opens the door towards electrolyte-gated low-voltage high- power tunable bulk resistors. It is further necessary to note that our findings are equally important to predict and understand potential induced conductivity changes in nanographene-based electrodes that are, for example, being extensively used in battery and supercapacitor applications.

2. Results and Discussion

2.1. Structural Characterization

The Brunauer-Emmett-Teller (BET) specific surface area (SSA) of highly activated BNG samples can be as high as 2800 m^2/g,[12] which is slightly higher than the specific surface area of single-layer graphene (2675 m^2/g).[21] The high surface area value demonstrates the presence of single-layer graphene flakes that are accessible from both sides by inert gas. However, unless otherwise stated, most measurements were performed on BNG samples with 1900 m^2/g specific surface area because recent theoretical results predict insufficient screening and thereby inefficient charge accumulation in single layer materials.[22] The BNG materials studied here are mechanically surprisingly robust given their extremely high BET surface area.[12,23] Deformation up to several percent strain is predominately elastic as revealed by both nanoindentation experiments[12] and macroscopic compression tests.[23] Even the highest surface area (i.e., lowest density) BNG materials (3189 m^2/g, ~150 kg/m^3) exhibit relatively high values for both Young's modulus E (ranging from 850 MPa when measured using nanoindentation[12] to 280 MPa measured by macroscopic compression tests[23]) and Meyer hardness (80 MPa, average contact pressure[12]). The mechanical robustness of BNG samples allows for rewetting the dry sample with electrolyte without any indication of mechanical deformation caused by pore collapse.

Results from structural analysis of a representative BNG sample through optical, scanning microscopy (SEM) and high-resolution transmission electron microscopy (HRTEM) are summarized in **Figure 1**a–c. Structural characterization by SEM (Figure 1b) and TEM (Figure 1c) reveals a multi-modal pore-size distribution with micron-sized macropores, few tens of nanometers wide meso-pores (more clearly seen in the two-dimensional cross sectional slices of the TEM tomogram, as shown in Figure S1, movie S1), and 1–2 nm sized micro pores between the individual graphene nanoleaflets. Owing to the limited contrast, the latter are not very clearly visible (refer to movies S1-S2). The individual graphene nanoleaflets are found to be tens of nanometers in size and have a twisted and intertwined appearance (Figure 1c). In HRTEM images mostly single-layer graphene nanoleaflets are observed in addition to a few double layer regions (Figure 1c). Multilayer regions are rarely found (one example is marked in Figure 1c) consistent with the large gravimetric surface area obtained by BET measurements.

The graphitic nature of BNG is further demonstrated by electron energy loss spectra (EELS) recorded at different regions in the diffraction mode; quite consistent spectra have been obtained and representative spectra are shown in Figure 1d–e. The low loss EEL spectrum shown in Figure 1(d) shows two plasmon excitation peaks at 5.2 eV (π plasmon) and 18.6 eV (coupled $\pi + \sigma$ plasmon), respectively. Due to the highly curved nature of the graphene layer in BNG, the π plasmon and the $\pi + \sigma$ plasmon include contributions from both in-plane (q || a) and out-of-plane modes (q || c). According to the simulation reported by Eberlein et al.,[24] the π plasmon mainly comes from the in-plane mode and the position of the maximum shift from 7 eV for graphite to 4.8 eV for single layer graphene; for the $\pi + \sigma$ plasmon, both in-plane mode and out-of-plane mode show considerable red shift when the structure changes from graphite to graphene. Especially the main peak of the in-plane excitation shifts from 27 eV for graphite to 15 eV for graphene. The simulation also suggests that for graphene bi-layers and tri-layers the maxima should appear between 15 eV and 20 eV, respectively. Therefore, the π and the $\pi + \sigma$ plasmon peaks of the BNG material show a small blue shift compared to single layer graphene and the positions actually matches better with bi- or tri-layer graphene sheets, consistent with the measured BET surface area (1900 m^2/g) from this sample. In addition, it may be noted that the extra blue shift in the plasmon peaks of the BNG material can result from a possible overlap between the individual but closely placed (a few times of the c lattice spacing in graphite) graphene flakes which can also shift the plasmon peaks towards the higher energy loss. On the other hand, the core-loss carbon

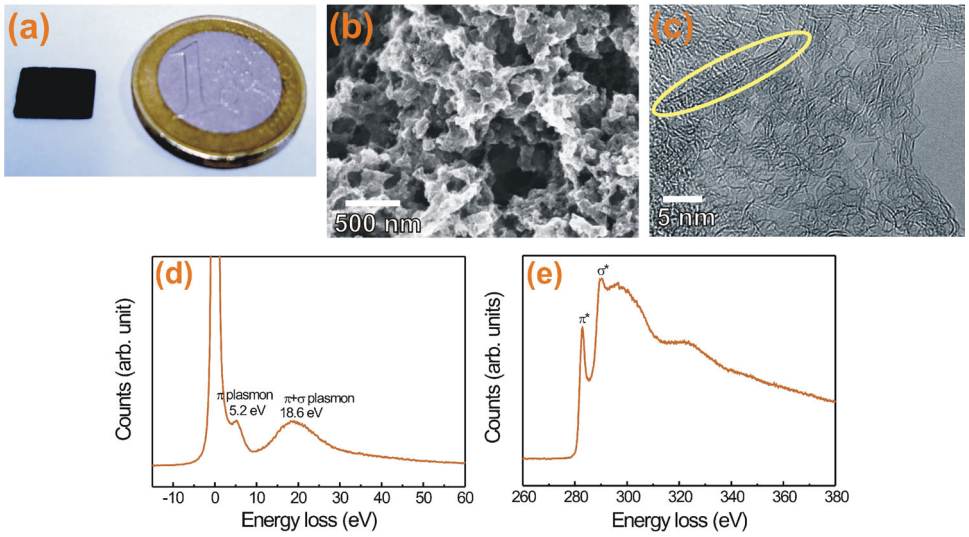

Figure 1. (a) Optical image of a piece of BNG used for the electrochemical and electrical measurements; (b) characteristic SEM image of the BNG material (SSA = 1900 m^2/g) demonstrating the hierarchical morphology of the material; (c) HRTEM image of BNG (SSA = 1900 m^2/g) showing mostly single or bi-layer nanographene sheets and a rare occurrence of flake with few layer graphenes (highlighted in yellow); (d) low loss EEL spectra recorded on BNG material with marked position of the π and $\pi + \sigma$ plasmon peaks; (e) core loss carbon K-edge spectra with typical graphite like fingerprint of exclusive sp^2 hybridization.

K-edge spectrum (Figure 1e) from the material is identical to that from the graphite, indicating exclusive sp^2 hybridization, which can be taken as the fingerprint of the fact that the material is solely comprised of graphene nanoleaflets.

2.2. Temperature-Dependent Electronic Transport

Temperature dependent conductivity measurements were performed to examine the electronic transport mechanism in BNG (**Figure 2**). The conductivity of BNG increases with increasing temperature and thus indicates a thermally activated hopping mechanism between localized states.[25] However, there seems to exit two clearly discernable regimes with different temperature dependence; at high temperatures, the conductivity follows an Arrhenius behavior (linear fit in Figure 2, solid line):

$$\ln(R) = \frac{E_A}{2K_B}\frac{1}{T} \quad (1)$$

At lower temperatures (<60 K), the change of resistivity becomes much slower than one can explain through a simple Arrhenius behavior. Instead the resistivity-temperature correlation can be fitted to a power law with the exponent $\gamma = \frac{1}{2}$, which is typically ascribed to a variable range hopping (VRH) mechanism:

$$\ln(R) = \left(\frac{T_0}{T}\right)^{\gamma} \quad (2)$$

Both transport mechanisms mentioned above seem to be feasible in the BNG materials studied here; for example, localized traps can be explained by heteroatoms or point defects, both of which are certainly present in our materials (e.g., Rutherford backscattering spectrometry (RBS) has confirmed the presence of trace amounts of hydrogen and oxygen impurities of 5% and 0.5%, respectively[12]). The VRH mechanism, on the other hand, can be explained by the small domain size of the graphitic building blocks revealed by EELS and TEM. It needs to be emphasized that the BNG materials discussed here are monolithic samples and do not contain binders or any other additives. Therefore, the temperature dependent resistivity behavior and the potential dependent conductivity changes (discussed below) are intrinsic properties and are related to the 3D morphology of the BNG materials.

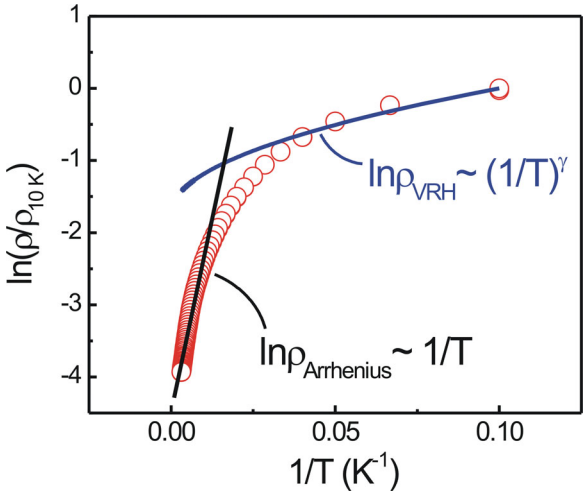

Figure 2. Temperature dependence of the electronic transport in BNG. The linear region at higher temperatures indicates an Arrhenius type activated transport, while the temperature dependence of the resistance at low temperatures can be best fitted by a power low with exponent $\gamma = \frac{1}{2}$, thus suggesting variable range hopping.

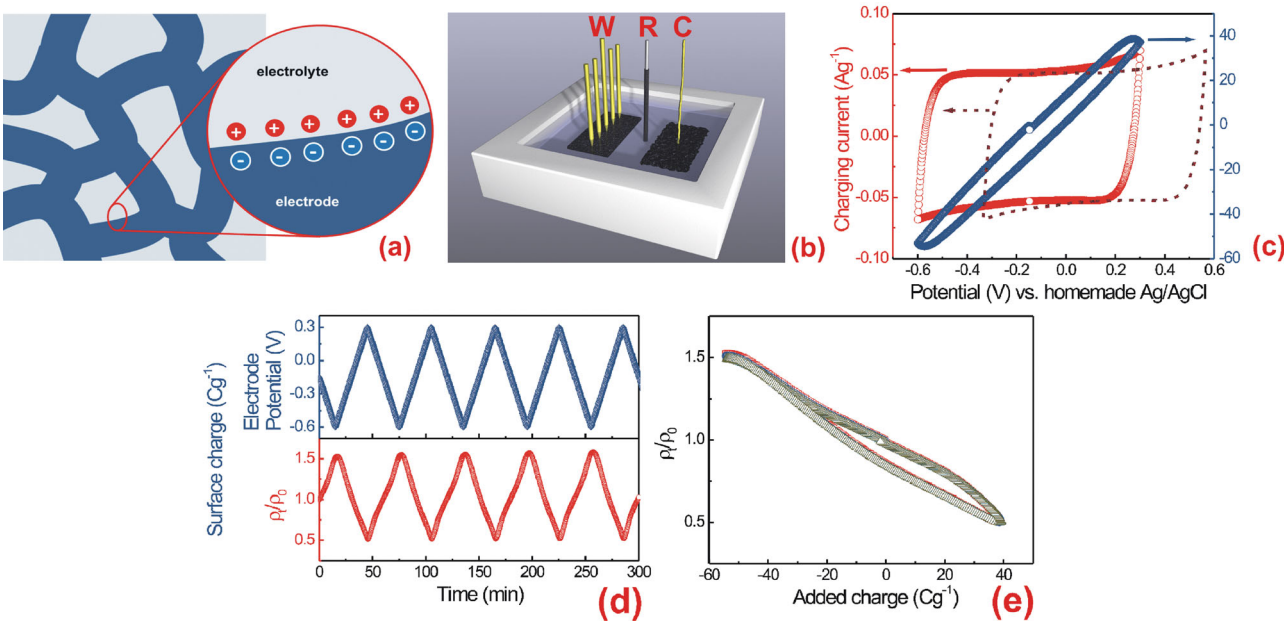

Figure 3. (a) Dynamic control of macroscopic properties in bulk materials can be achieved by applying the concept of electrolyte-gating to nanoporous materials; electrochemical polarization of the electrode/electrolyte interface of an electrolyte impregnated nanoporous bulk material induces a change in the charge carrier concentration which, for example, can lead to macroscopic conductivity modulations; (b) experimental setup for the electrochemical characterization and potential dependent resistivity measurements; W, R and C stand for the BNG working electrode (SSA = 1900 m^2/g, sample dimensions $10 \times 5 \times 1$ mm^3), the homemade Ag/AgCl reference electrode and the Kynol carbon cloth as counter electrode, respectively; (c) CV curves recorded for a 900 mV potential window (–0.6 V to 0.3 V vs. homemade Ag/AgCl) using a scan rate of 0.5 mV/s and the corresponding surface charge density, the dotted line represents the position of the cyclic-voltammetry with respect to standard Ag/AgCl reference electrode;[26] (d) simultaneous in-situ 4-point probe resistivity measurement with respect to the applied potential showing a completely reversible variation of a few hundred percent; (e) the same resistivity modulation replotted with respect to the added change density to the BNG electrode.

2.3. Surface Charge-Induced Conductivity Modulation

Electrochemical potential induced conductivity changes were studied using a BNG sample as the working electrode in a three-electrode electrochemical cell while simultaneously monitoring the resistance of the BNG material with a 4-point probe measurement setup. The interfacial charging mechanism is schematically shown in **Figure 3**a, and details of the in-situ 4-point probe measurement setup are shown in Figure 3b. A representative cyclic voltammetry (CV) curve (recorded during an in-situ electrical measurement) within the potential window of –0.6 V to 0.3 V, vs. our homemade Ag/AgCl reference electrode[26] is shown in Figure 3c. The rectangular shape of the CV curve (Figure 3c) is characteristic for an ideally polarizable electrode within the capacitive potential region and thereby ensures the absence of specific ion adsorption and faradaic currents. The closed surface charge curve further confirms the absence of parasitic currents. This is consistent with the observation that both the CV curves and the simultaneously recorded resistivity variations are completely reversible (Figure 3c,d). It is important to note that even upon further widening the potential window no significant chemisorption can be noticed thus demonstrating the chemical inertness of the BNG electrodes. In absence of specific ion adsorption or faradaic currents, the resistance modulation of the BNG electrode (Figure 3d) can be attributed to field-induced carrier injection/depletion. As revealed by Figure 3d,e, within the potential window of –0.6 V to 0.3 V vs. homemade Ag/AgCl, the resistivity of the BNG working electrode increases during the negative potential scans (i.e., addition of negative charge/electrons to the system) and decreases during the positive potential scans (i.e., addition of positive charge/holes to the system).

This monotonic increase in resistivity with decreasing electrode potential is an unexpected result as the Fermi level of un-doped graphene coincides with the Dirac point, i.e., one would expect that the resistivity decreases for both charging directions as the density of states (DOS) increases with increasing distance from the Dirac point. A possible explanation of the measured resistivity behavior is that our BNG material is heavily p-doped; filling of the unoccupied conduction band states during negative sweeps thus then increases the resistivity. Indeed, *p*-doping is quite commonly found even in pristine graphene material that is either mechanically exfoliated[27] or chemically derived.[19,28,29] It is also consistent with the presence of some residual oxygen in our BNG samples detected in RBS measurements.[12]

The variation of the resistivity as a function of the accumulated surface charge is shown in Figure 3e. The accumulated surface charge has been calculated from the measured charging/discharging currents (Figure 3c) using the assumptions that (1) there are no parasitic faradaic currents and (2) there is negligible charge build up at the open circuit potential (OCP) which is quite a reasonable assumption for a weakly adsorbing electrolyte at low concentrations. The fact that

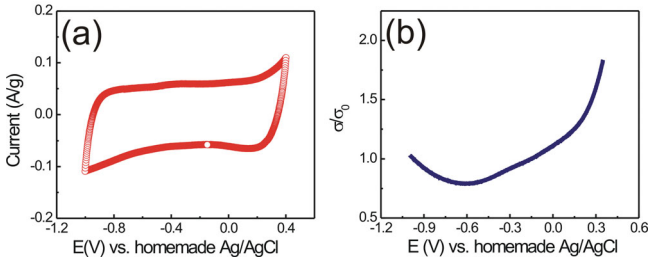

Figure 4. (a) CV recorded for a potential window of –1.0 to 0.4 V vs. homemade Ag/AgCl reference, with a scan rate of 0.5 mV/s; (b) corresponding conductivity measurement, the data measured during the anodic scan between -1.0 V to 0.4 V.

the conductivity of the BNG electrode at the OCP is identical to that of the dry sample further corroborates insignificant charge build up at OCP. As can be seen from Figure 3e, the total change in the charge carrier density of the BNG electrode, combining the charge accumulation and the charge depletion is ~100 C/g, or ~0.01 e/C atom. Interestingly, this is two orders of magnitude larger than the intrinsic carrier concentration of un-doped graphite, which is about 10^{-4} e/C atom.[30] This value, however, needs to be regarded as the lower boundary of the real carrier density of BNG electrodes as the presence of any point defects or curvature has been shown to strongly increase the density of states at the Dirac point;[22] both types of defects are definitely present in our material, most likely even in relatively high concentrations, as suggested by the intertwined, curved appearance of the graphene sheets in high resolution TEM images (Figure 1c). Moreover, the relatively small change in resistivity by only a factor of 4 (Figure 3d,e), observed between two extreme potentials, suggests that the surface charge induced increase in carrier density is accompanied by a simultaneous drop in the carrier mobility.

Figure 4 shows that a shallow conductivity minimum/resistivity maximum around –0.6 V (vs. homemade Ag/AgCl[26] is observed when the potential window is further widened towards negative values (from –0.6 V to –1.0 V vs. homemade Ag/AgCl.[26] The conductivity minimum has been observed quite reproducibly for different samples between –0.6 V to –0.7 V (see for example, Figure S2). If this conductivity minimum is indeed a consequence of the DOS minimum at the Dirac point, the following conclusions can be made: (a) the BNG material is heavily *p*-doped (possibly due to oxygen impurities) as the charge neutrality point (–0.6 V vs. homemade Ag/AgCl[26]) is always found at a higher negative potential with respect to the OCP (around –0.15 V vs. homemade Ag/AgCl[26]); the charge build up on the BNG electrode at the OCP is assumed to be insignificant; (b) the conductivity of the BNG at the OCP (i.e., at zero electrochemical surface charge) seems to be hole-dominated which is a reasonable assumption as the conductivity in pristine graphene is usually hole-dominated.[29,30] For example, following a similar electrolyte-gating (e.g., ionic liquid,[18] ion-gel[19] or polymer electrolyte[20]) approach, large positive gate potentials (i.e., similar to a large negative potential on the BNG electrode in the present case) have always been necessary to reach to the charge neutrality point in both single-layer[18,20] and tens of micron thick graphene sheets;[19] (c) the large change in carrier concentration is probably at least partially compensated by a significant decrease in carrier mobility upon charge injection, thus explaining the experimentally observed relatively small ρ_{max}/ρ_{min} ratio. For example, it is well-known that the carrier mobility of un-doped and clean graphene sheets at the charge neutrality point can be many thousands of centimeters-square per volt-second, but decreases dramatically with injection of charged carriers.[31] In fact, this is the primary reason for the low On-Off current ratio obtained in graphene based GFETs (always <10) even with the electrolyte-gating approach where the carrier concentration can be altered by orders of magnitude; (d) the shallowness of the conductivity minimum observed for the BNG material (Figure 4, Figure S2) is most likely related to the high level of *p*-doping in the pristine material. Previous studies have shown similar results, i.e. that the conductivity minimum becomes broader and shallower with increasing concentration of charged impurities.[31,32]

To estimate the kinetics of electrochemical-surface charge induced conductivity changes in BNG, the potential was pulsed between –0.6 V and 0.3 V (vs. homemade Ag/AgCl) while simultaneously monitoring the charging/discharging currents and the resistivity of the BNG electrode. The time dependence of the applied electrode potential, charging currents, added charge into the BNG electrode and the resulting resistance change are compared in **Figure 5**. Both the added charge (Figure 5c) and the resulting resistivity modulations (Figure 5d) were highly reproducible. The mass-specific charge density stored in the system can be calculated from Figure 5c and exceeds 125 F/g. The exponential decay fit for one of such charging cycles (data taken between 25–35 min in Figure 5c,d) and the corresponding resistivity alteration are shown in Figure S3. Exponential fits yield very similar relaxation times for the charging current ($\tau_1 = 50$ s) and the resistivity changes ($\tau_2 = 57$ s) thus further confirming the correlation between both. The experimentally observed characteristic charging time ($\tau = RC$; *R*, electrolyte resistance; *C*, total capacitance) is qualitatively consistent with the value that can be calculated using the total capacitance (1.4 F) of the 11.1 mg BNG block, working-to-counter electrode distance (about 1 cm) and the typical conductivity of the used aqueous electrolytes (around 10^{-1} S/cm). This assumes a parallel plate capacitor geometry, where τ is independent of the electrode size. This simple approximation, however, is not valid for nanoporous BNG electrodes where τ can be expected to increase with increasing electrode size/mass due to an increase in the diffusion length of the ions inside the nanopores. Nevertheless, considering the bulk conductivity and the bulk density of the material to be around 3.5 S/cm and 200 mg/cm^3, respectively, it is possible to estimate that in a sheet of BNG material of about 100 µm thickness and a few cm^2 apparent surface area would easily support a current over 1 kA for an applied potential of 1 V. Hence, even a 100 µg BNG electrode should be capable of delivering a power of 1 kW at a drive voltage of 1 V and its output power can be tuned reversibly with a small gate potential. The reaction time of such power tunable bulk resistor/transistors can be reduced to a few seconds or even less depending on the position of the counter electrode which can easily be placed at a much closer proximity than it is in the present case.

The findings described in this study may equally apply to other recently developed graphene macroassemblies that are made from graphene oxides.[33,34] The On/Off ratio may even be higher when they are made from less defective graphene building blocks that have a lower carrier density at the Dirac

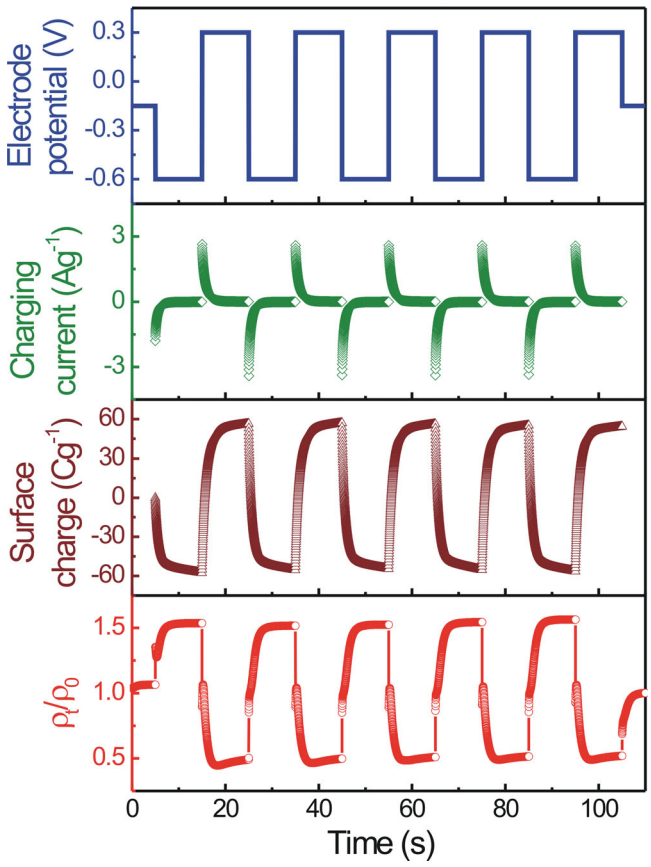

Figure 5. Electrochemical and resistivity response of the BNG sample with respect to the potential pulses. Applied potential pulses between –0.6 V and 0.3 V with respect to homemade Ag/AgCl reference electrode (blue); the charging current normalized to unit mass (green); variation in the added charge in the system per unit mass (wine) and corresponding change in the measured resistivity (red) is plotted (from top-to-bottom) versus time.

point. Finally, although we have not reproduced our experiments with non-aqueous electrolytes which generally allow for a wider adsorption-free, capacitive potential window, it can be speculated that the conductivity would continue to increase further with increasing charge accumulation/depletion which would be beneficial for the device power performance. In the perspective of supercapacitor applications, it is important to note that the conductivity of these graphene-based materials always stays high enough and never become the limiting factor for the device power performance.

Finally, it is worthwhile to mention that the electrolyte-gating induced resistivity modulations reported here are most likely connected to the recently reported macroscopic strain effects with reversible volume strain amplitudes up to 6.6%.[23] The kinetics of both the resistivity modulations reported here and the strain modulations reported earlier[23] closely follow the charge-discharge kinetics of the BNG electrodes, thus suggesting that both phenomena are fundamentally linked to the interfacial charge density. Thus the large electrolyte-gating induced carrier density modulation reported in this study seems also to affect the C-C interatomic bonding thus leading to a macroscopic strain response.

3. Conclusion

We have demonstrated electrochemical surface charge induced resistivity modulations in monolithic, nanoporous bulk graphene materials. The material has a hierarchical pore architecture that combines an ultra-high surface area associated with micro-pores for effective charge injection/depletion with a macro-porous morphology that enables fast ion transport. The sp^2 hybridization of the carbon skeleton consisting of intertwined single and double layer graphene nanoleaflets have been confirmed by TEM/EELS. At high temperatures, the charge transport in this material is governed by activated hopping, whereas at lower temperature, the temperature dependence can be better described by a variable range hopping mechanism. The high electrochemical EDL capacitance of BNG opens doors to the deterministic and reversible control of its resistivity using electrolyte-gating. The time constant for these resistivity modulations is reasonably small and in combination with the large conductivity of the material one can imagine high power bulk resistor/transistor applications where the power output can easily be tuned with less than one volt gate potential.

4. Experimental Section

The BNG material was prepared through carbonization and thermal activation of porous polymer monoliths, as previously described.[12] Specifically, resorcinol and formaldehyde were polymerized in an aqueous solution, using glacial acetic acid as the catalyst. The reaction mixture was then cured at 70 °C for 72 h, resulting in the formation of an orange polymeric gel. After drying under ambient conditions, the resultant polymer foam was carbonized at 1050 °C for 3 h under an N_2 atmosphere, yielding a porous carbon monolith with a density of ~550 kg/m^3. Activation of the carbon foam (2 cm × 3 cm × 4 mm, 1.2 g) to generate the BNG electrode was carried out under flowing CO_2 (10 sccm) at 950 °C for up to 5 h. The BNG electrodes used for the present study were characterized for structural and morphological aspects using scanning (Leo 1530 Gemini) and transmission electron microscopy using a FEI Titan 80–300 electron microscope. The TEM sample was prepared by grinding the BNG material in a mortar and subsequent ultrasonic dispersion of the resulting powder in ethanol. A drop of the dispersion was then placed onto a Cu grid coated with holey carbon film (2 nm). The TEM images and the EELS spectra were taken from the sample part that is free standing across such holes. The electron microscope was operated at 80 kV to avoid any knock-on beam damage in carbon. High-resolution transmission electron microscopy (HRTEM) enabled direct observation of the graphene layers. Electron energy-loss spectroscopy (EELS) was performed with Tridiem Gatan image filter (GIF 863). The EEL spectra were recorded on a few tens of nanometers wide area by focusing the beam on the edge part of a few flakes. The low-loss EEL spectra were used to evaluate the average number of graphitic layers in the BNG sample by using the energy position of the $\pi + \sigma$ plasmon feature. The energy-loss near edge structure (ELNES) of the carbon K edge was acquired to confirm the dominant sp^2 hybridization. Furthermore, in order to study the porous structure, electron tomography was carried out in TEM mode by acquiring tilt series images, the reconstruction of which were calculated by Inspect3D and the 3D volume was visualized by Amira.

The electrochemical measurements were performed by using an Autolab PGSTAT-302 potentiostat, with a standard three-electrode electrochemical cell and using homemade Ag/AgCl reference electrodes. The BNG sample was used as the working electrode and very high surface area carbon cloth (kynol) as the counter. Macroscopic four-point resistance measurements were performed (using a Keithley 6221 current source and a Keithley 2182 nanovoltmeter) in-situ

while the potential of the BNG was either varied continuously with constant scan rate cyclovoltammetry or was pulsed back-and-forth using chronoamperometric mode. For electrochemical and electrical measurements a rectangular piece of BNG sample (as shown in Figure 1a) with 11.1 mg sample mass was used. All electrochemical and electrical measurements are performed at room temperature unless otherwise stated. An aqueous solution of 0.1 M sodium perchlorate ($NaClO_4$) in deionized water was used as the electrolyte.

The in-situ electrical measurements were performed using the typical four-point resistance measurement setup as shown in Figure 3b; a constant current of 5 mA was allowed to flow through the BNG material using the outer contacts and the potential drop across the inner contacts was continuously monitored. The middle contact was used to connect the BNG monolith to the potentiostat as the working electrode. Although the charging currents (Figure 3c) were order of magnitude lower than the currents applied across the BNG block, the distance between the contact electrodes were carefully kept constant in order to avoid any transient current effects.

Homemade Ag/AgCl reference electrodes were prepared by coating Ag-wires with AgCl by applying an electrode potential of 1 V (with respect to pure silver electrode) for 60 s, using 1 M HCl solution. The Ag/AgCl electrodes were then washed thoroughly with copious amounts of de-ionized water and a small cut was made at the tip of the electrodes (Ag/AgCl wires) in order to expose pure silver. These homemade reference electrodes can show stable potential for sufficiently long time of use and can be very helpful for miniature electrochemical cells where positioning or incorporating commercial Ag/AgCl electrodes is quite difficult. The potential of six home made Ag/AgCl electrodes were measured with respect to standard Ag/AgCl reference, for a duration of 48 hours, where all the homemade reference electrodes showed a very stable potential, over the entire period. However, each of them had an offset of –0.265 V versus the standard Ag/AgCl reference (c(KCl) = 3 mol/L, Metrohm GmbH).

The temperature dependent conductivity measurement was performed using a physical property measurement system (PPMS) from Quantum Design.

Supporting Information

Supporting Information is available from the Wiley Online Library or from the author.

Acknowledgements

The authors acknowledge the financial support by the Deutsche Forschungsgemeinschaft (DFG) under contract HA1344/25–1. SD and HH also thank the financial support from Helmholtz Gemeinschaft in the form of Helmholtz Virtual Institute VI530. Work at LLNL was performed under the auspices of the US DOE by LLNL under Contract DE-AC52–07NA27344. Project 12-ERD-035 was funded by the LDRD Program at LLNL.

Received: October 15, 2013
Revised: November 25, 2013
Published online: February 3, 2014

[1] J. Bardeen, W. H. Brattain, *Phys. Rev.* **1949**, *75*, 1208–1225.
[2] W. Shockley, *Bell System Technical Journal* **1949**, *28*, 435–489.
[3] K. Dawon, *Technical memorandum issued by Bell Labs*, **1961**.
[4] S. Roberts, *Phys Rev.* **1947**, *71*, 890–895.
[5] J. Weissmüller, R. N. Viswanath, D. Kramer, P. Zimmer, R. Würschum, H. Gleiter, *Science* **2003**, *300*, 312–315.
[6] M. Weisheit, S. Fähler, A. Marty, Y. Souche, C. Poinsignon, D. Givord, *Science* **2007**, *315*, 349–351.
[7] L.-H. Shao, M. Ruther, S. Linden, S. Essig, K. Busch, J. Weissmüller, M. Wegener, *Adv. Mater.* **2010**, *22*, 5173–5177.
[8] S. Dasgupta, R. Kruk, D. Ebke, A. Hütten, C. Bansal, H. Hahn, *J. Appl. Phys.* **2008**, *104*, 103707.
[9] S. Dasgupta, M. Lukas, K. Dössel, R. Kruk, H. Hahn, *Phys. Rev. B* **2009**, *80*, 085425.
[10] M. Sagmeister, U. Brossmann, S. Landgraf, R. Würschum, *Phys. Rev. Lett.* **2006**, *96*, 156601.
[11] S. Dasgupta, G. Stoesser, N. Schweikert, R. Hahn, S. Dehm, R. Kruk, H. Hahn, *Adv. Funct. Mater.* **2012**, *22*, 4909–4919.
[12] J. Biener1, S. Dasgupta, L. Shao, D. Wang, M. A. Worsley, A. Wittstock, J. R. I. Lee, M. M. Biener, C. A. Orme, S. O. Kucheyev, B. C. Wood, T. M. Willey, A. V. Hamza, J. Weissmüller, H. Hahn, T. F. Baumann, *Adv. Mater.* **2012**, *24*, 5083–5087.
[13] S. Parida, D. Kramer, C. A. Volkert, H. Rösner, J. Erlebacher, J. Weissmüller, *Phys. Rev. Lett.* **2006**, *97*, 035504.
[14] A. Wittstock, J. Biener, M. Bäumer, *Phys. Chem. Chem. Phys.* **2010**, *12*, 12919–12930.
[15] J. Biener, A. Wittstock, T. F. Baumann, J. Weissmüller, M. Bäumer, A. V. Hamza, *Materials* **2009**, *2*, 2404–2428.
[16] L. H. Qian, M. W. Chen, *Appl. Phys. Lett.* **2007**, *91*, 083105.
[17] Y. Ohno, K. Maehashi, Y. Yamashiro, K. Matsumoto, *Nano Lett.* **2009**, *9*, 3318–3322.
[18] F. Chen, Q. Qing, J. Xia, J. Li, N. Tao, *J. Am. Chem. Soc.* **2009**, *131*, 9908–9909.
[19] B. J. Kim, S.-K. Lee, M. S. Kang, J.-H Ahn, J. H. Cho, *ACS Nano* **2012**, *6*, 8646–8651.
[20] A. Das, S. Pisana, B. Chakraborty, S. Piscanec, S. K. Saha, U. V. Waghmare, K. S. Novoselov, H. R. Krishnamurthy, A. K. Geim, A. C. Ferrari, A. K. Sood, *Nature Nanotechnology* **2008**, *3*, 210–215.
[21] C. Liu, Z. Yu, D. Neff, A. Zhamu, B. Z. Jang, *Nano Lett.* **2010**, *10*, 4863–4868.
[22] B. C. Wood, T. Ogitsu, M. Otani, J. Biener, *J. Phys. Chem. C* **2014**, *118*, 4–15.
[23] L.-H. Shao, J. Biener, H.-J. Jin, M. M. Biener, T. F. Baumann, J. Weissmüller, *Adv. Funct. Mater.* **2012**, *22*, 3029–3034.
[24] T. Eberlein, U. Bangert, R. R. Nair, R. Jones, M. Gass, A. L. Bleloch, K. S. Novoselov, A. Geim, P. R. Briddon, *Phys. Rev. B* **2008**, *77*, 233406.
[25] M. Y. Han, J. C. Brant, P. Kim, *Phys. Rev. Lett.* **2010**, *104*, 056801.
[26] All the electrochemical potentials referred in this study is measured with respect to homemade Ag/AgCl reference electrodes (for preparation, see experimental) which show an offset of –0.265 V vs. standard Ag/AgCl reference electrode (c(KCl) = 3 mol/L, Metrohm GmbH).
[27] Z. Chen, Y.-M. Lin, M. J. Rooks, P. Avouris, *Physica E* **2007**, *40*, 228–232.
[28] X. Li, X. Wang, L. Zhang, S. Lee, H. Dai, *Science* **2008**, *319*, 1229–1232.
[29] X. Wang, Y. Ouyang, X. Li, H. Wang, J. Guo, H. Dai, *Phys. Rev. Lett.* **2008**, *100*, 206803.
[30] M. S. Dresselhaus, G. Dresselhaus, *Adv. Phys.* **1981**, *30*, 139–326.
[31] Y.-W. Tan, Y. Zhang, K. Bolotin, Y. Zhao, S. Adam, E. H. Hwang, S. Das Sarma, H. L. Stormer, P. Kim, *Phys. Rev. Lett.* **2007**, *99*, 246803.
[32] S. Adam, E. H. Hwang, V. M. Galitski, S. Das Sarma, *Proc. Natl. Acad. Sci. USA* **2007**, *104*, 18392–18397.
[33] M. A. Worsley, P. J. Pauzauskie, T. Y. Olson, J. Biener, J. H. Satcher, Jr., T. F. Baumann, *J. Am. Chem. Soc.* **2010**, *132*, 14067–14069.
[34] M. A. Worsley, T. Y. Olson, J. R. I. Lee, T. M. Willey, M. H. Nielsen, S. K. Roberts, P. J. Pauzauskie, J. Biener, J. H. Satcher Jr., T. F. Baumann, *J. Phys. Chem. Lett.* **2011**, *2*, 921–925.